APPENDIX

TOR-mediated Ypt1 as an autophagy determinant regulates the stepwise assembly of ATG proteins

Weijing Yao[#], Yuting Chen[#], Yingcong Chen[#], Pengwei Zhao[#], Jing Liu, Yi Zhang, Qiang Jiang, Yu Xie, Siyu Fan, Miao Ye, Yigang Wang, Yuyao Feng, Choufei Wu, Xue Bai, Mingzhu Fan, Shan Feng, Juan Wang, Yixian Cui, Hongguang Xia, Cheng Ma, Zhiping Xie, Liqin Zhang, Qiming Sun, Wei Liu, Cong Yi*

[#]Co-first author

[*] Correspondence: Cong Yi, email: yiconglab@zju.edu.cn.

Table of Contents

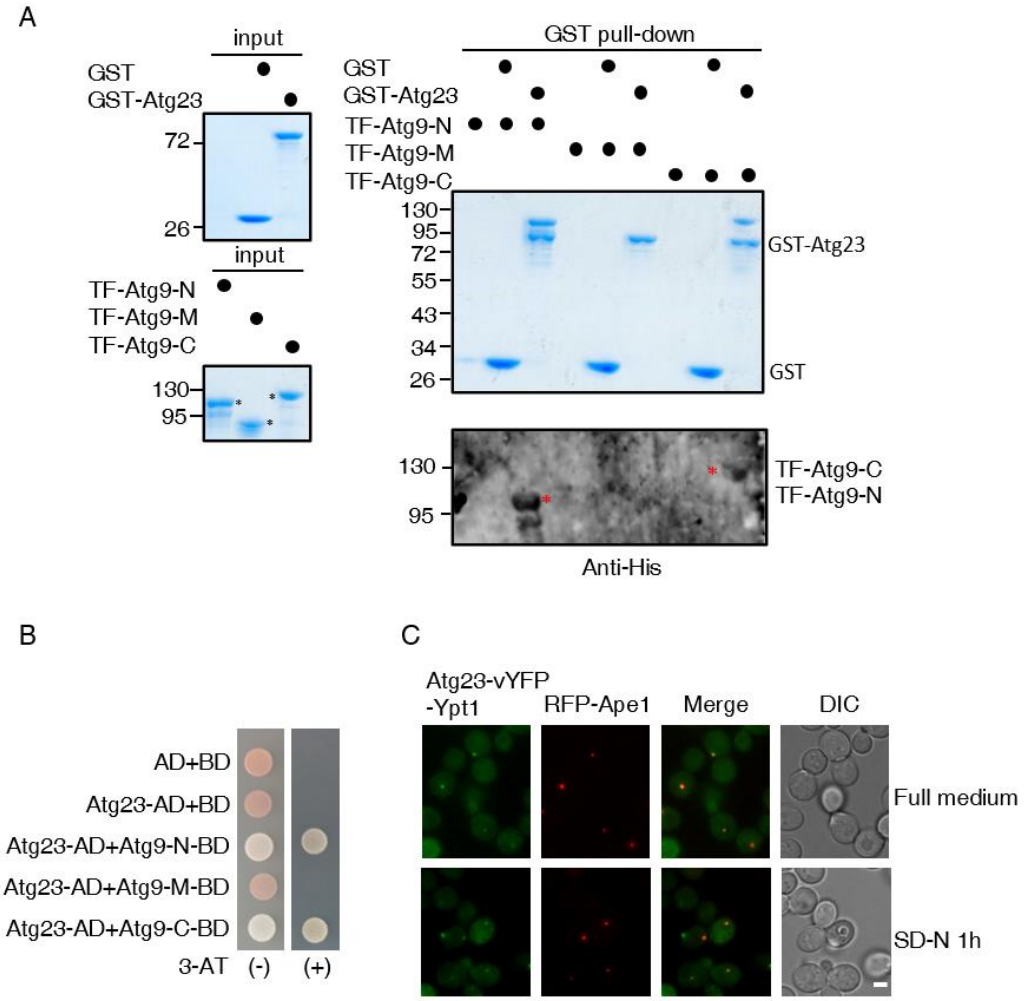

Appendix Figure S1. Atg23 binds directly to Atg9-N and Atg9-C.

(A) GST pulldowns were performed using purified His_6-tagged TF-Atg9 N (2-318aa), TF-Atg9 M (395-534aa), or TF-Atg9 C (747-997aa) with GST or GST-Atg23 from *E. coli*. Protein samples were separated by SDS-PAGE, and then detected using Coomassie blue staining. The asterisk represents the target protein.

(B) The AH109 strain was transformed with plasmids expressing AD-fused with Atg23 and plasmids expressing BD-fused with Atg9-N (2-318aa), Atg9-M (395-534aa), or Atg9-C (747-997aa). These strains were grown on SD-Leu-Trp or SD-His-Leu-Trp (3-AT) agar plates at 30°C for 3 d.

(C) Representative fluorescence microscopy images of WT cells expressing the BiFC constructs Atg23-VN, VC-Ypt1, and RFP-Ape1 cultured in SD and shifted to SD-N for 1 h. Scale bar: 2 μm.

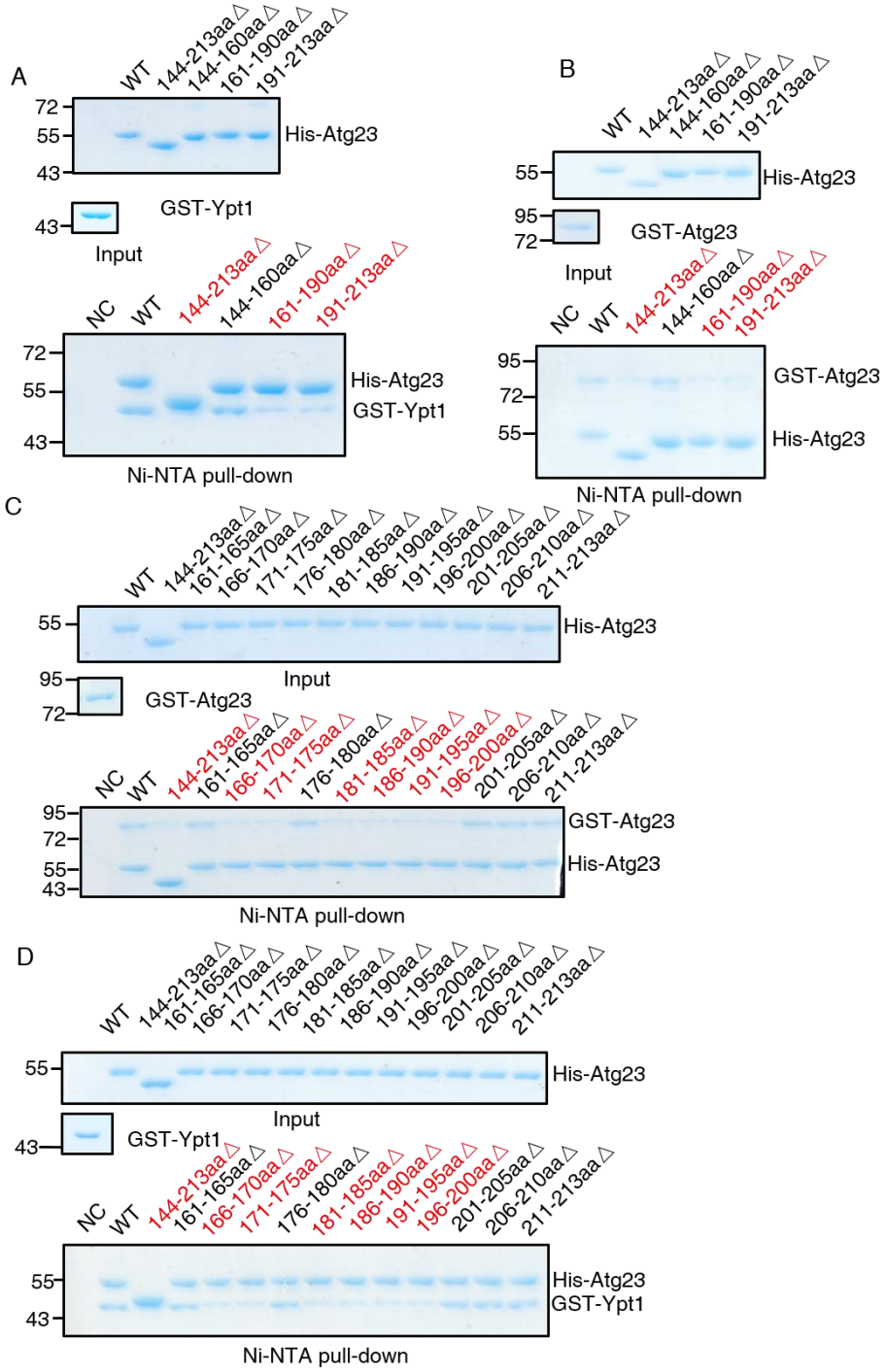

Appendix Figure S2. The dimerization of Atg23 is a prerequisite for its binding to Ypt1.

(A-D) Ni-NTA pulldowns were performed using purified GST-Ypt1(A, D) or GST-Atg23(B, C) with His-Atg23 or the indicated His-Atg23 variants from *E. coli*. Protein samples were separated by SDS-PAGE, and then detected using Coomassie blue staining.

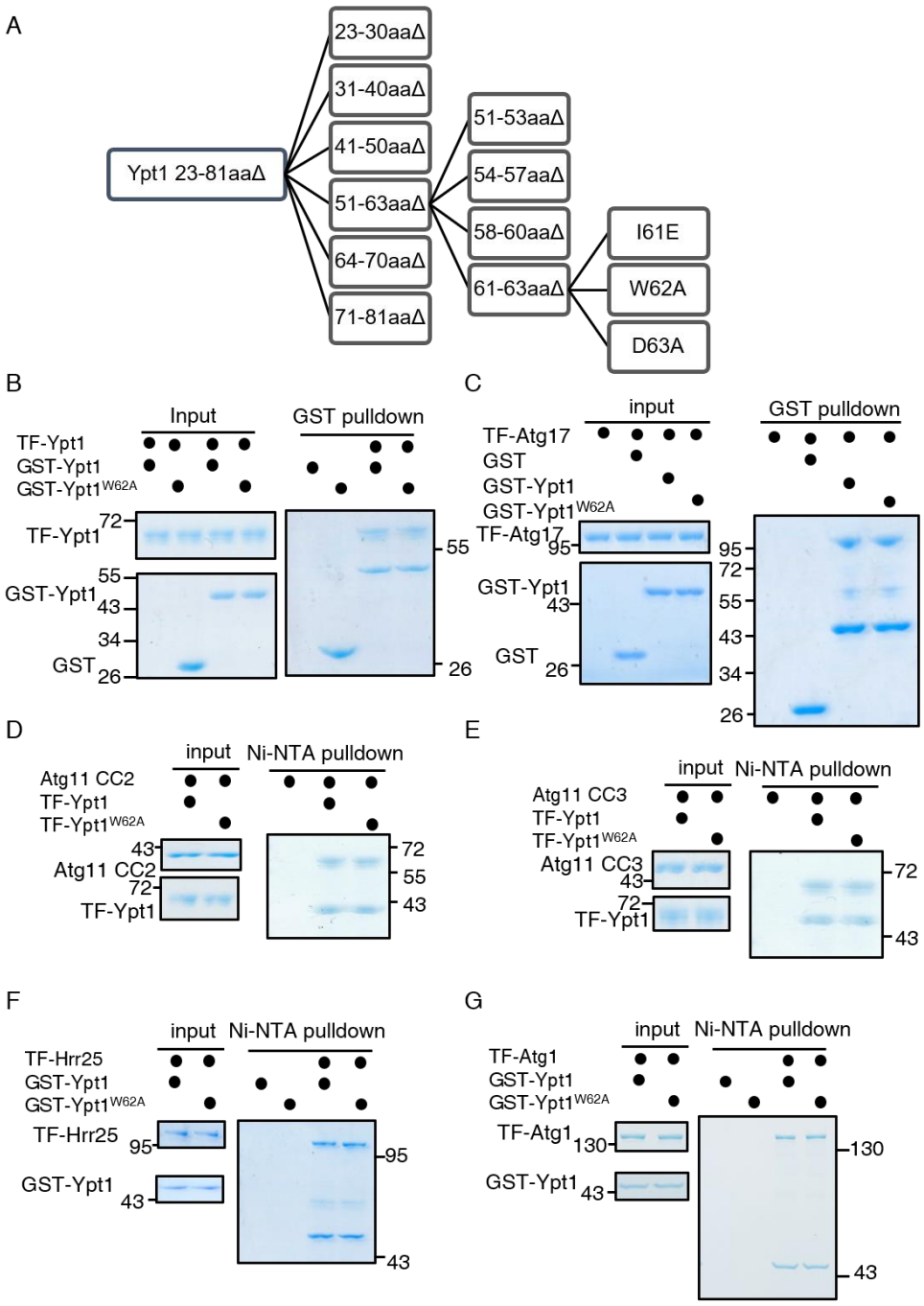

Appendix Figure S3. ***Ypt1*^{W62A} does not impair its association with Atg1, Atg17, Atg11, Hrr25, as well as its dimerization.**

(A) The scheme for identifying key amino acid residues binding to Atg23 on Ypt1 by BiFC assays. Since Ypt1 S22 residue is GDP-bound form of Ypt1 and Ypt1 ^{S22N} mutant blocked the binding of Ypt1 to Atg23, we did not test this mutant.

(B, C) GST pulldowns were performed using purified GST-Ypt1 or GST-Ypt1^{W62A} with TF-Ypt1(B) or TF-Atg17(C) from *E. coli*. Protein samples were separated by SDS-

PAGE, and then detected using Coomassie blue staining.

(D, E) Ni-NTA pulldowns were performed using purified TF-Ypt1 or TF-Ypt1^{W62A} with Atg11 CC2(D) or CC3 domain(E) from *E. coli*. Protein samples were separated by SDS-PAGE, and then detected using Coomassie blue staining.

(F, G) Ni-NTA pulldowns were performed using purified GST-Ypt1 or GST-Ypt1^{W62A} with TF-Atg1(F) or TF-Hrr25(G) domain from *E. coli*. Protein samples were separated by SDS-PAGE, and then detected using Coomassie blue staining.

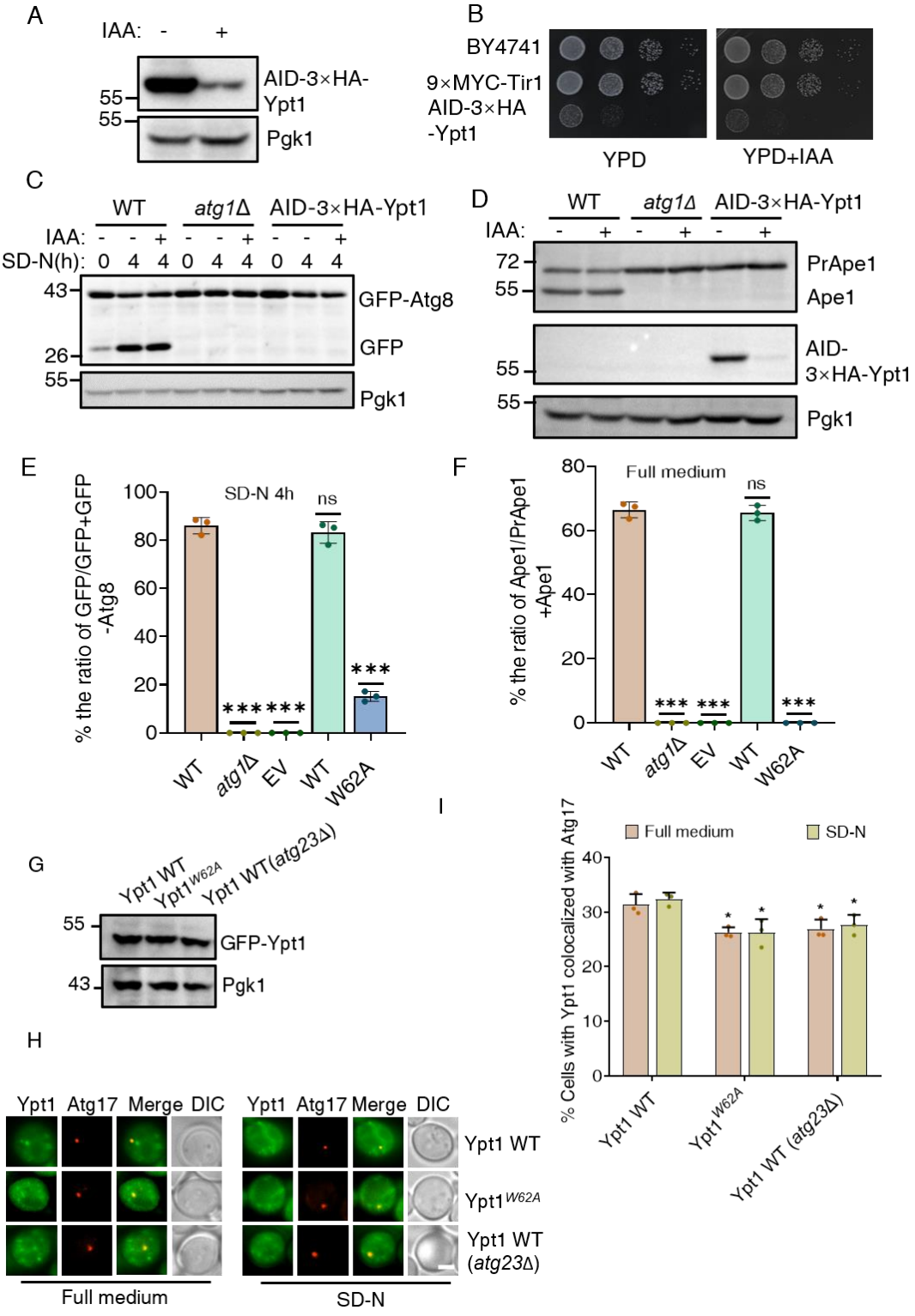

Appendix Figure S4. Ypt1 W62 residue is required for autophagy and the Cvt pathway, and the PAS recruitment of Ypt1 does not rely on the binding of Ypt1-Atg23 to any great extent.

(A) Cells expressing AID-3×HA-Ypt1 were grown to log phase, and then subjected to

0.5 mM IAA treatment for 0 h or 2 h, the expression of AID-3×HA-Ypt1 was detected by anti-HA antibody. Pgk1 served as a loading control.

(B) Wild-type cells (BY4741), cells expressing 9×MYC-TIR1 or co-expressing 9×MYC-TIR1 and AID-3×HA-Ypt1 were grown on YPD or YPD+0.5 mM IAA agar plate for 2 days at 30°C.

(C) Cells co-expressing GFP-Atg8 and Vph1-mCherry in wild-type, *atg1*Δ, or AID-3×HA-Ypt1 yeast strains were treated with DMSO or IAA for 2h, and then subjected to SD-N in the presence or absence of IAA for 4h. Autophagic activity was analyzed by western blot for GFP-Atg8 cleavage. Pgk1 served as a loading control.

(D) Wild-type, *atg1*Δ, or AID-3×HA-Ypt1 yeast strains were treated with DMSO or 0.5mM IAA for 2h under nutrient-rich conditions. The activity of the Cvt pathway was analyzed by western blot for the maturation of PrApe1. Pgk1 served as a loading control.

(E) The cleavage of GFP-Atg8 from Figure 3E were quantified and presented as mean ± SD (n=3). ***p < 0.001; NS, no significance; two-tailed Student's t tests were used.

(F) The maturation of PrApe1 from Figure 3F were quantified by the ratio of Ape1/PrApe1+Ape1 and presented as mean ± SD (n=3). ***p < 0.001; NS, no significance; two-tailed Student's t tests were used.

(G) AID-3×HA-Ypt1 yeast cells co-expressing GFP-Ypt1 or GFP-Ypt1^{W62A} with Atg17-2×mCherry or AID-3×HA-Ypt1 *atg23*Δ yeast cells co-expressing Atg17-2×mCherry with GFP-Ypt1 were grown to log phase, and then subjected to 0.5 mM IAA treatment for 2 h. The expression of GFP-Ypt1 or GFP-Ypt1^{W62A} were detected using anti-GFP antibody. Pgk1 served as a loading control.

(H) The yeast strains from (G) were treated with DMSO or IAA for 2h, and then subjected to SD-N in the presence or absence of IAA for 0h or 1h. Images of cells were obtained using an inverted fluorescence microscope. Scale bar, 2 μm.

(I) Cells from (H) were quantified for the number of cells in which GFP-Ypt1 or GFP-Ypt1^{W62A} colocalized with Atg17-2×mCherry. n=300 cells were pooled from three independent experiments. Data are shown as mean ± SD. *p < 0.05; two-tailed Student's t tests were used.

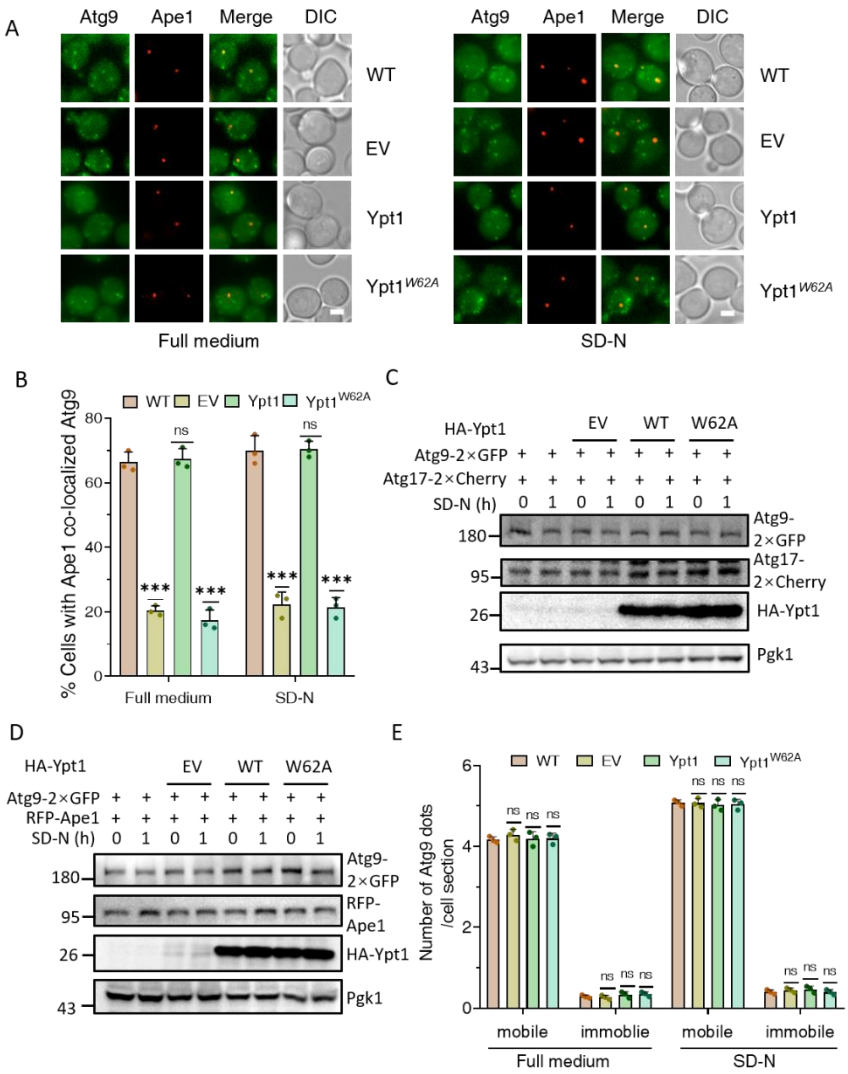

Appendix Figure S5. Ypt1^{W62A} impaired the PAS recruitment of Atg9 vesicles, but did not affect the biogenesis of Atg9 vesicles

(A) Wild type yeast strains co-expressing RFP-Ape1 and Atg9-2×GFP or AID-3×HA-Ypt1 yeast strains co-expressing RFP-Ape1 and Atg9-2×GFP transformed with empty vector, FLAG-Ypt1, or FLAG-Ypt1^{W62A} plasmids were grown to log phase, 0.5mM IAA was added to degrade endogenous AID-3×HA-Ypt1 for 2h, and then subjected to SD-N for 0h or 1h. Images of cells were obtained using the inverted fluorescence Microscope. Scale bar, 2 μm.

(B) Cells from (A) were quantified for the number of cells in which Atg9-2×GFP colocalized with RFP-Ape1. n=300 cells were pooled from three independent experiments. Data are shown as mean ± SD. ***p < 0.001; ns, no significance; two-

tailed Student's t tests were used.

(C-D) The protein samples from Fig 4A(C) and EV2A(D) were analysis by western-blot using the corresponding antibody. Pgk1 served as a loading control.

(E) Formation of mobile Atg9 vesicles was not affected by Ypt1^{W62A}. Cells from Figure 4A were subjected to IAA for 2h to degrade endogenous Ypt1, then subjected to nitrogen starvation for 0 h and 1 h. Images were analyzed by time-lapse microscopy at 30 ms/frame using an inverted microscope (Nikon-STORM/A1R). Scale Bar: 2 μm. The number of mobile Atg9 puncta and immobile Atg9 puncta per cell section ($n > 300$) was counted with Imaris 9.3.1. and presented as mean ± SD (n=3). NS, no significance; two-tailed Student's t tests were used.

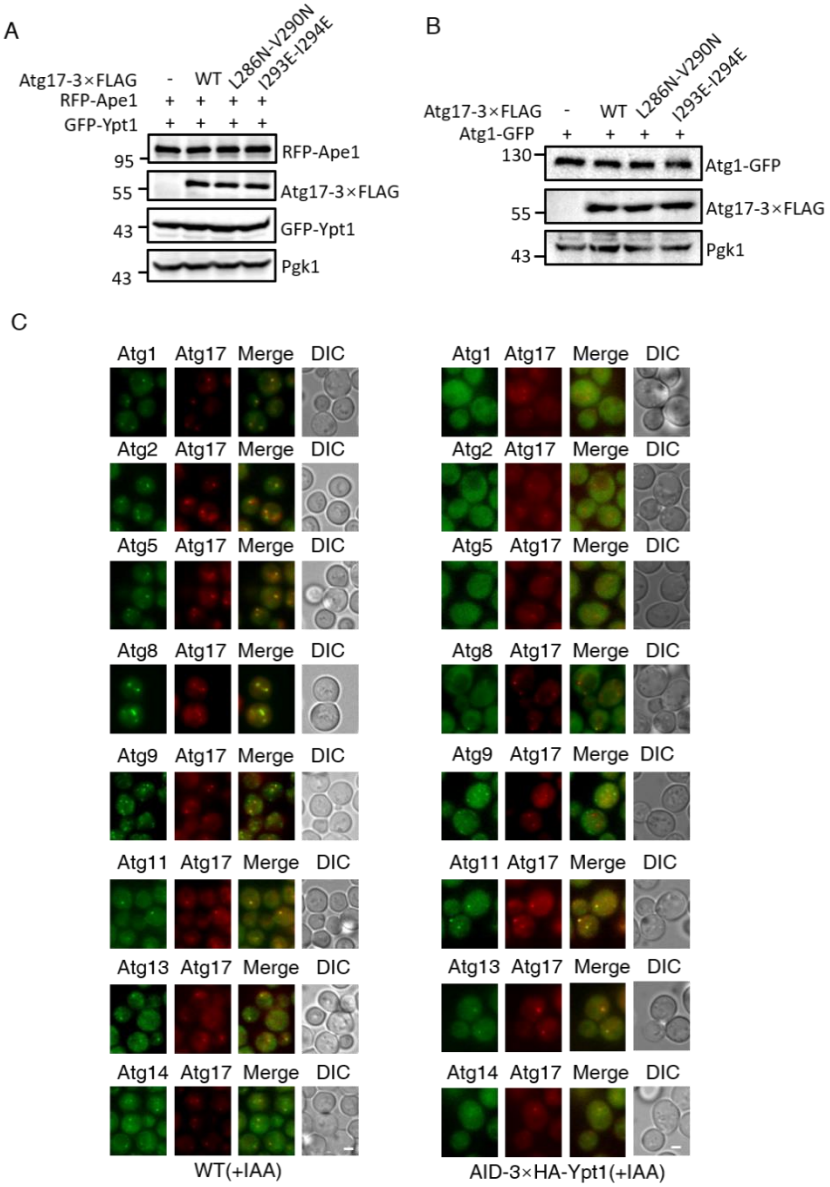

Appendix Figure S6. The image data of the PAS recruitment of ATG proteins under the degradation of Ypt1.

(A, B) The protein samples from Figure 5F or 5H were analysis by western-blot using the corresponding antibody. Pgk1 served as a loading control.

(C) WT or AID-3×HA-Ypt1 yeast strains co-expressing Atg17-2×mCherry and the indicated GFP-tagged ATG proteins were grown to early log phase, IAA was then added to induce the degradation of AID-3×HA-Ypt1 for 2h. These yeast cells were then subjected to nitrogen starvation with IAA treatment for 1h. Images were obtained by the inverted fluorescence microscopy. Scale bar: 2 μm.

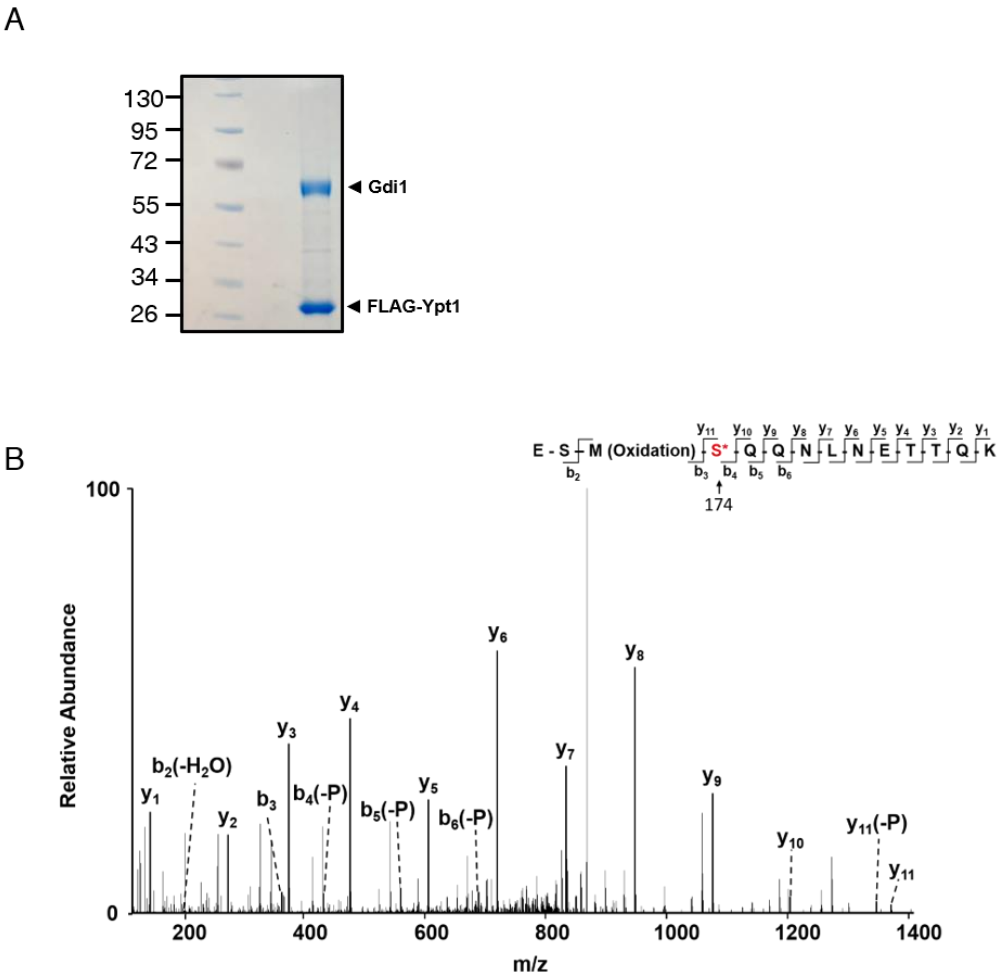

Appendix Figure S7. MS identified that Ypt1 W62 residue was phosphorylated.

(A) FLAG-Ypt1 is purified by using anti-FLAG nanobody beads under nutrient-rich medium.

(B) FLAG-Ypt1 was separated by SDS-PAGE. The phosphorylation site was then identified using LC-MS/MS.

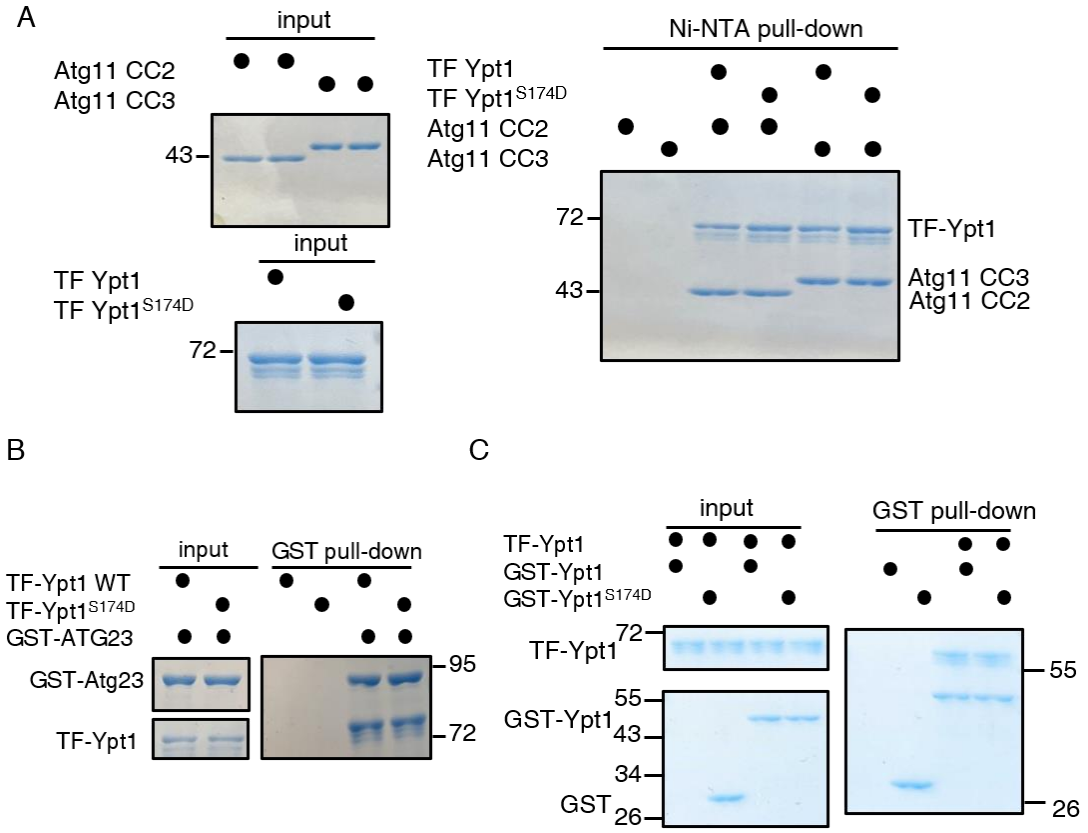

Appendix Figure S8. *Ypt1^{S174D}* does not impair Ypt1 association with Atg11, Atg23, or its dimerization.

(A) Ni-NTA pulldowns were performed using purified TF-Ypt1 or TF-Ypt1^{S174D} with Atg11 CC2 or CC3 from *E. coli*. Protein samples were separated by SDS-PAGE, and then detected using Coomassie blue staining.

(B) GST pulldowns were performed using purified TF-Ypt1 or TF-Ypt1^{S174D} with GST-Atg23 from *E. coli*. Protein samples were separated by SDS-PAGE, and then detected using Coomassie blue staining.

(C) GST pulldowns were performed using purified GST-Ypt1 or GST-Ypt1 ^{S174D} with TF-Ypt1 from *E. coli*. Protein samples were separated by SDS-PAGE, and then detected using Coomassie blue staining.

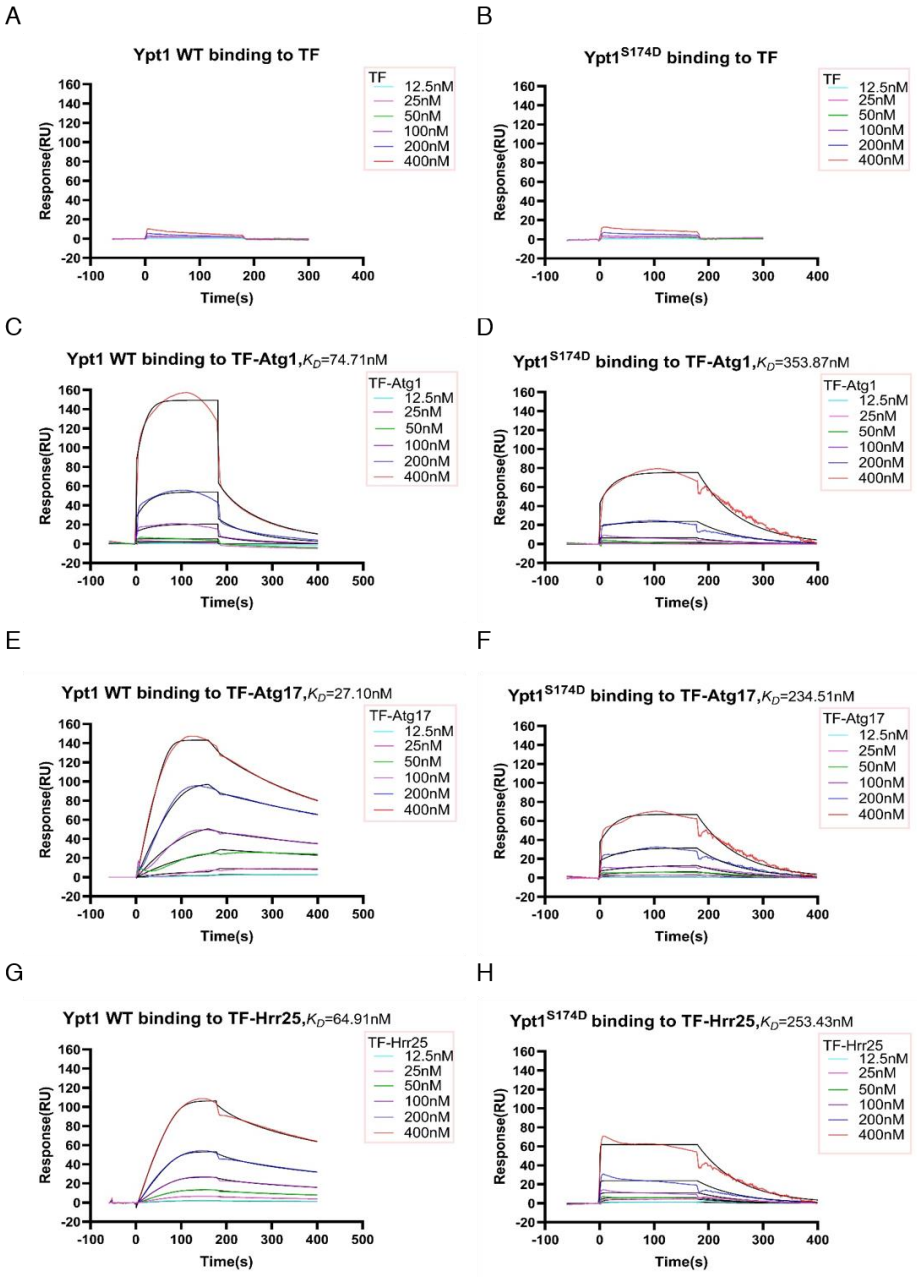

Appendix Figure S9. *Ypt1^{S174D}* significantly impair its association with Atg1, Atg17, or Hrr25 *in vitro*. Purified recombinant proteins GST-Ypt1 WT or GST-Ypt1^{S174D} were covalently immobilized on the sensor chip via their amine groups and purified recombinant proteins TF, TF-Atg1, TF-Atg17, or TF-Hrr25 flowed over the GST-Ypt1 WT or S174D. TF, TF-Atg1, TF-Atg17, or TF-Hrr25 proteins were diluted to the indicated concentrations (from 12.5nM to 400nM) before injected. The results were fit to a 1:1 binding model. Each time, five different protein concentrations were used for calculating the K_D values.

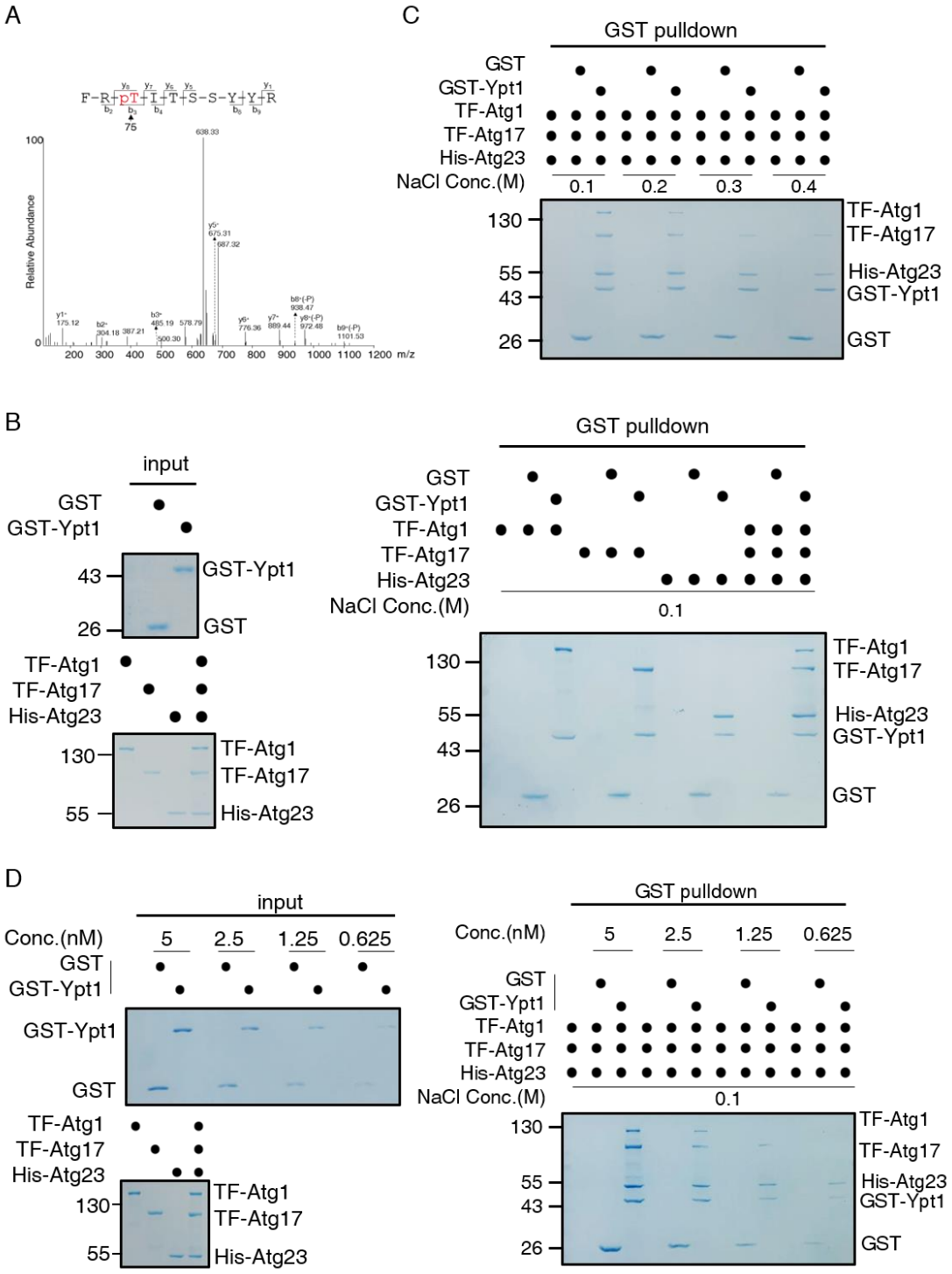

Appendix Figure S10. MS identified that Rab1 T75 is phosphorylated, and the binding of Atg1, Atg17, and Atg23 with Ypt1 are competitive.

(A) Identification of Rab1 T75 phosphorylation by means of liquid chromatography–mass spectrometry (LC-MS)/MS analysis.

(B) GST pulldowns were performed using GST or GST-Ypt1 with TF-Atg1, TF-Atg17,

and His_6-Atg23 from *E. coli* in the washing buffer containing 100mM NaCl. Protein samples were separated by SDS-PAGE, and then detected using Coomassie blue staining.

(C) GST pulldowns were performed using GST or GST-Ypt1 with TF-Atg1, TF-Atg17, and His_6-Atg23 from *E. coli* in the washing buffer containing the indicated concentrations of NaCl. Protein samples were separated by SDS-PAGE, and then detected using Coomassie blue staining.

(D) GST pulldowns were performed using TF-Atg1, TF-Atg17, andHis_6-Atg23 with the indicated concentrations of GST or GST-Ypt1 with from *E. coli* in the washing buffer containing 100mM NaCl. Protein samples were separated by SDS-PAGE, and then detected using Coomassie blue staining.